Sensor Fault Detection of Small Turboshaft Engine for Helicopter

Sangman Seong, Ihnseok Rhee
Korea University of Technology and Education
Hyeok Ryu
Korea Aerospace Research Institute

Abstract

Most of engine control systems for helicopter turboshaft engines are equipped with dual sensors. For the system with dual redundancy, analytic methods are used to detect faults based on the system dynamical model. Helicopter engine dynamics are affected by aerodynamic torque induced from the dynamics of the main rotor. In this paper an engine model including the rotor dynamics is constructed for the T700-GE-700 turboshaft engine powering UH-60 helicopter. The singular value decomposition(SVD) method is applied to the developed model in order to detect sensor faults. The SVD method which do not need an additional computation to generate residual uses the characteristics that the system outputs in direction of the left singular vector if an input is applied in direction of the right singular vector. Simulations show that the SVD method works well in detecting and isolating the sensor faults.

Nomenclature

N_P : rotational speed of power turbine, rpm
N_G : rotational speed of gas generator, rpm
P_3 : station 3 total pressure, psi
T_{45} : station 4.5 temperature, degR
W_f : fuel flow, lbm/sec
J : moment of inertia of power turbine and associated accessories, ft-lbf-sec^2
Q_{GT}: torque produced by compressor/ gas-generator, lbf-ft
Q_{PT}:torque produced by power turbine, lbf-ft
Q_{req}: external torque to engine, lbf-ft
Q_{mr} : main rotor torque, lbf-ft
n_e : gear ratio
Ω_{mr} : rotational speed of main rotor, rad/sec
Ω_T : design rotational speed of main rotor, rad/sec
e_H : ratio of flapping and lagging hinge location and blade length
ω_f : undamped natural frequency of flapping motion, rad/sec
ζ_f : damping ratio of flapping motion
ω_l : undamped natural frequency of lagging motion, rad/sec
ζ_l : damping ratio of lagging motion

1. Introduction

Gas turbine engines have been used for propulsion systems of fixed wing and rotary wing aircraft. Recent high performance gas turbine engine is controlled by a full authority digital engine control(FADEC) system. Because a mechanical backup system is not employed for the engine equipped with FADEC a failure of FADEC system makes the engine uncontrollable and thereby causes the loss of aircraft. Hence the fault tolerance against FADEC failure is very important.

Most of engine control systems for helicopter turboshaft engines are equipped with dual sensors. For the system with dual redundancy, analytic methods are used to detect faults based on the system dynamical model. The dynamics of small turboshaft engines are described by power turbine rotational speed and gas generator rotational speed. While the gas generator speed is independent of the power turbine speed the dynamics of power turbine are coupled with the gas generator speed and affected by external

torque.[1] The external torque for helicopter is due to main rotor, tail rotor, and associated accessories. The aerodynamic load induced from the rotor dynamics is the main source of external torque and only a small portion of external torque is produced by parts other than the main rotor. The main rotor dynamics consists of flapping and lagging motion of blades.[2] In this paper an engine model including rotor dynamics is constructed for the T700-GE-700 turboshaft engine powering UH-60 helicopter.

Since FADEC system under consideration has dual redundancy, analytic(or model based) methods are used to detect and isolate faults. The model based fault detection methods can be divided into three categories: parity method, parameter estimation method, and observer based method[3]. These methods require the calculation of the residuals from the input output data. Recently, the authors proposed a new fault detection method which utilize the SVD of the frequency response of the system and applied it to the FADEC system which included engine system only[4]. When the system input is sinusoidal, this method has advantage in the point that it does not require calculating residuals. In this paper, we use the SVD based method to detect sensor fault for our FADEC system which considers both engine and rotor systems.

2. System Models

In this paper we consider a UH60 Helicopter described in ref. 5. The UH60 is powered by two T700-GE-700 turboshaft engines. Fig. 1 shows interaction between engine and helicopter rotor system. Power turbine angular velocity, N_P and acceleration, $\dot{N}_P$ are fed to the rotor system through gearbox. Torque required to rotate the rotor with Ω_{mr} and $\dot{\Omega}_{mr}$ acts as an external torque to engine. It is assumed that tail rotor and accessories consume 10% of main rotor torque. Constant $2\pi/60$ is introduced to convert RPM unit to rad/sec unit. The engine model and the main rotor model adopted in this paper are

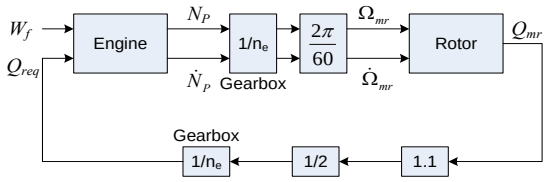

Fig. 1 Engine and rotor interaction

presented in ref. 1 and ref. 5, respectively. Those are implemented in forms of SIMULINK blocks.

The combined model is to be linearized along a trim point in order to apply fault detection scheme. A trim condition has to be found for the combined model. In the rotor model motion of each blade is considered. Since each blade never reaches steady state, a trim for the rotor is not found in general sense but in sense of average over 1 revolution of rotor. Hence trim conditions for rotor and engine are calculated separately.

2.1 Rotor Model

At trim condition, the main rotor is assumed to rotate with designed rotor speed, Ω_T. At given flight condition, we can find collective pitch angle, cyclic pitch angles which leads to trim in sense of average. Ω_{mr} and $\dot{\Omega}_{mr}$ are perturbed respectively along the trim and rotor torque, Q_{mr} is measured. A linear model can be obtained from the measured Q_{mr} by applying the modified maximum likelihood parameter estimation(MMLE) technique[6].

Flight condition considered is hovering at sea level in standard atmosphere with total weight of 16825lbf . At trim

$$\Omega_{mr} = 27 \text{ rad/s}, \quad Q_{mr} = 35323 \text{ lbf-ft} \qquad (1)$$

Fig. 2 depicts the measured Q_{mr} when pulse input of Q_{mr} with 0.5rad/sec amplitude from 2sec to 4sec and pulse input of $\dot{Q}_{mr}$ with 0.5rad/sec^2 amplitude from 6sec to 8sec are applied to the helicopter hovering at sea level in standard atmosphere. Because the rotor dynamics are

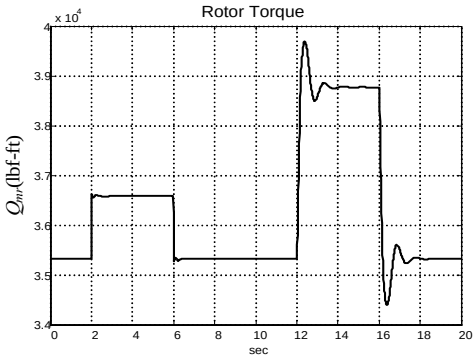

Fig. 2 Q_{mr} Measurement due to pulse input of Ω_{mr} and $\dot{\Omega}_{mr}$

governed by flapping and lagging motion, we can describe the rotor model with observer canonical form[7] :

$$\begin{bmatrix}\dot{x}_{f1}\\ \dot{x}_{f2}\\ \dot{x}_{l1}\\ \dot{x}_{l2}\end{bmatrix} = \underbrace{\begin{bmatrix}0 & -\omega_f^2 & 0 & 0\\ 1 & -2\zeta_f\omega_f & 0 & 0\\ 0 & 0 & 0 & -\omega_l^2\\ 0 & 0 & 1 & -2\zeta_l\omega_l\end{bmatrix}}_{A_r} \underbrace{\begin{bmatrix}x_{f1}\\ x_{f2}\\ x_{l1}\\ x_{l2}\end{bmatrix}}_{x_r} + \begin{bmatrix}b_{11} & b_{12}\\ b_{21} & b_{22}\\ b_{31} & b_{32}\\ b_{41} & b_{42}\end{bmatrix}\begin{bmatrix}\Delta\Omega_{mr}\\ \Delta\dot{\Omega}_{mr}\end{bmatrix} \quad (2)$$

$$\Delta Q_{mr} = \underbrace{[0\ 1\ 0\ 1]}_{C_r}\boldsymbol{x}_r + [d_1\ 0]\begin{bmatrix}\Delta\Omega_{mr}\\ \Delta\dot{\Omega}_{mr}\end{bmatrix} \quad (3)$$

The undamped natural frequencies of flapping and lagging motion are given by[5]

$$\omega_f = \Omega_T\sqrt{1+\frac{3}{2}e_H}, \qquad \omega_l = \Omega_T\sqrt{\frac{3}{2}e_H}$$

For the UH60, $\omega_f = 29.93\,\mathrm{rad/sec}$, $\omega_l = 7.14\,\mathrm{rad/sec}$. By using MMLE we obtain

$$\zeta_f = 0.345,\ \zeta_l = 0.395,\ d_1 = 2518$$

$$\begin{bmatrix}b_{11} & b_{12}\\ b_{21} & b_{22}\\ b_{31} & b_{32}\\ b_{41} & b_{42}\end{bmatrix} = \begin{bmatrix}-65745.6 & 768708\\ 2270.66 & -22764.5\\ 3830.15 & 307809\\ 633.74 & 29754.6\end{bmatrix}$$

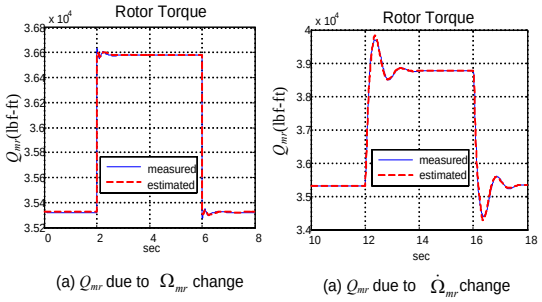

Fig. 3 Rotor parameter estimation results

Fig. 3 compares the measured Q_{mr} denoted by solid line with the estimated Q_{mr} from the linear model (2) and (3) denoted by dotted line. Fig. 3(a) shows Q_{mr} perturbed by pulse input of Ω_{mr} and fig. 3(b) perturbed by pulse input of $\dot{\Omega}_{mr}$.

2.2 Engine Model

T700-GE-700 Turboshaft engine shown in fig. 4 is composed of compressor, combustor, gas generator, and power turbine. Reference 3 describes T700-GE-700 engine dynamics with 5 state variables: gas generator speed, power turbine speed, and 3 pressures in compressor and gas generator. For the rotor and the engine to be in trim, from fig. 1

$$N_P = \frac{60}{2\pi}n_e\Omega_{mr}, \quad Q_{req} = \frac{1.1\,Q_{mr}}{2n_e} \quad (4)$$

A trim condition of engine is calculated with equation (4) where Ω_{mr} and Q_{mr} are the quantities at the rotor trim.

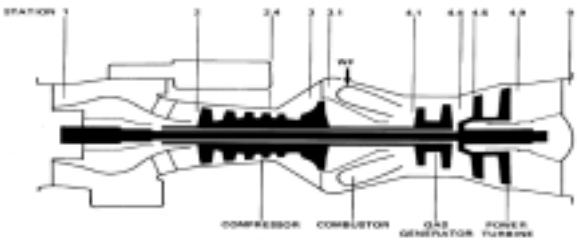

Fig. 4 Turboshaft engine

Linearized model along a trim condition has 5 state variable as mentioned above. However the dynamics of pressure can be neglected since pressure variables has much faster dynamics than gas generator and power turbine rotational speeds for a small turboshaft engine such as T700-GE-700.[5] In addition the gas generator speed, N_G is independent of the power turbine speed, N_P. Hence the linearized engine model is obtained as follows :

$$\dot{\boldsymbol{x}}_e = \boldsymbol{A}_e \boldsymbol{x}_e + \boldsymbol{B}_e W_f - \begin{bmatrix} \frac{60}{2\pi}\frac{\Delta Q_{req}}{J} \\ 0 \end{bmatrix} \quad (5)$$

where $\boldsymbol{x}_e = [\Delta N_P \ \Delta N_G]^T$,

$$\boldsymbol{A}_e = \frac{60}{2\pi}\begin{bmatrix} \frac{1}{J}\frac{\partial Q_{PT}}{\partial N_P} & \frac{1}{J}\frac{\partial Q_{PT}}{\partial N_G} \\ 0 & \frac{1}{J_G}\frac{\partial Q_{GT}}{\partial N_G} \end{bmatrix}$$

$$\boldsymbol{B}_e = \frac{60}{2\pi}\begin{bmatrix} \frac{1}{J}\frac{\partial Q_{PT}}{\partial W_f} & \frac{1}{J}\frac{\partial Q_{GT}}{\partial W_f} \end{bmatrix}^T$$

For a given flight condition,

$$\boldsymbol{A}_e = \begin{bmatrix} -1.565 & 2.240 \\ 0 & -2.934 \end{bmatrix}, \quad \boldsymbol{B}_e = \begin{bmatrix} 121540 \\ 117543 \end{bmatrix}$$

Eigen values are -1.565 and -2.934 which are related to N_P and N_G, respectively. Note that rotor flapping and lagging motions are much faster than the gas generator speed and power turbine speed.

If N_P, N_G, P_3, and T_{45} are chosen to be measured, then measurement equation are

$$\underbrace{\begin{bmatrix} \overline{N}_P \\ \overline{N}_G \\ \overline{P}_3 \\ \overline{T}_{45} \end{bmatrix}}_{\bar{\boldsymbol{y}}} = \underbrace{\begin{bmatrix} 0.00478 & 0 \\ 0 & 0.00224 \\ 0 & 0.01395 \\ 0 & -0.06478 \end{bmatrix}}_{\boldsymbol{C}_e} \boldsymbol{x}_e + \underbrace{\begin{bmatrix} 0 \\ 0 \\ 319.61 \\ 6581.6 \end{bmatrix}}_{\boldsymbol{D}_e} W_f \quad (6)$$

where bars on the variables denote measured values of associated variables and units of $\overline{N}_P$ and $\overline{N}_G$ are percent of designed values.

2.3 Combined Model

From fig. 1

$$\Delta Q_{req} = \frac{1.1}{2n_e}\Delta Q_{mr}, \ \Delta \Omega_{mr} = \frac{2\pi}{60}\frac{\Delta N_p}{n_e} \quad (7)$$

Combing equations (3), (5) and (7) yields

$$\dot{\boldsymbol{x}}_e = \widetilde{\boldsymbol{A}}_e \boldsymbol{x}_e + \boldsymbol{B}_e W_f + \widetilde{\boldsymbol{C}}_r \boldsymbol{x}_r \quad (8)$$

where

$$\widetilde{\boldsymbol{A}}_e = \boldsymbol{A}_e - \begin{bmatrix} \frac{1.1 d_1}{2J n_e^2} & 0 \\ 0 & 0 \end{bmatrix}, \ \widetilde{\boldsymbol{C}}_r = \begin{bmatrix} -\frac{66}{4\pi J n_e}\boldsymbol{C}_r \\ \boldsymbol{0} \end{bmatrix}$$

Equation (2) can be rewritten as

$$\dot{\boldsymbol{x}}_r = \boldsymbol{A}_r \boldsymbol{x}_r + \boldsymbol{B}_{r1}\boldsymbol{x}_e + \boldsymbol{B}_{r2}\dot{\boldsymbol{x}}_e \quad (9)$$

where

$$\boldsymbol{B}_{r1} = \frac{2\pi}{60 n_e}\begin{bmatrix} b_{11} & 0 \\ b_{21} & 0 \\ b_{31} & 0 \\ b_{41} & 0 \end{bmatrix}, \ \boldsymbol{B}_{r2} = \frac{2\pi}{60 n_e}\begin{bmatrix} b_{12} & 0 \\ b_{22} & 0 \\ b_{32} & 0 \\ b_{42} & 0 \end{bmatrix}$$

Combining (8) and (9) we obtain a complete model :

$$\begin{bmatrix} \boldsymbol{I} & \boldsymbol{0} \\ -\boldsymbol{B}_{r2} & \boldsymbol{I} \end{bmatrix}\begin{bmatrix} \dot{\boldsymbol{x}}_e \\ \dot{\boldsymbol{x}}_r \end{bmatrix} = \begin{bmatrix} \widetilde{\boldsymbol{A}}_e & \widetilde{\boldsymbol{C}}_r \\ \boldsymbol{B}_{r1} & \boldsymbol{A}_r \end{bmatrix}\begin{bmatrix} \boldsymbol{x}_e \\ \boldsymbol{x}_r \end{bmatrix} + \begin{bmatrix} \boldsymbol{B}_e \\ \boldsymbol{0} \end{bmatrix} W_f \quad (10)$$

Equation (10) is a 6-th order system. As mentioned earlier, rotor state is much faster than engine state. Neglecting the dynamics of rotor state we can reduce the order of equation (9) to second order. Substituting $\dot{\boldsymbol{x}}_r = 0$ into (2) and (3) yields

$$\Delta Q_{mr} = \frac{\partial Q_{mr}}{\partial \Omega_{mr}}\Delta \Omega_{mr} + \frac{\partial Q_{mr}}{\partial \dot{\Omega}_{mr}}\Delta \dot{\Omega}_{mr} \quad (11)$$

where

$$\frac{\partial Q_{mr}}{\partial \Omega_{mr}} = \frac{b_{11}}{\omega_f^2} + \frac{b_{31}}{\omega_l^2} + d_1,$$

$$\frac{\partial Q_{mr}}{\partial \dot{\Omega}_{mr}} = \frac{b_{12}}{\omega_f^2} + \frac{b_{32}}{\omega_l^2}$$

Substituting (7) and (11) into (5) we obtain the reduced model as follows :

$$\boldsymbol{R}_e \dot{\boldsymbol{x}}_e = \hat{\boldsymbol{A}}_e \boldsymbol{x}_e + \boldsymbol{B}_e W_f \qquad (12)$$

where $\boldsymbol{R}_e = \begin{bmatrix} 1 & \frac{1.1}{2Jn_e^2}\frac{\partial Q_{mr}}{\partial \dot{\Omega}_{mr}} \\ 0 & 1 \end{bmatrix}$ and

$$\hat{\boldsymbol{A}}_e = \boldsymbol{A}_e - \frac{1.1}{2Jn_e^2}\begin{bmatrix} 0 & \frac{\partial Q_{mr}}{\partial \Omega_{mr}} \\ 0 & 0 \end{bmatrix}$$

For a hovering flight condition considered here

$$\frac{\partial Q_{mr}}{\partial \Omega_{mr}} = 2510.7, \quad \frac{\partial Q_{mr}}{\partial \dot{\Omega}_{mr}} = 6907.6$$

Fig. 5 shows the responses of full nonlinear model, linearized model (10), and reduce order linearized model (12) for a pulse input of fuel flow.

3. Fault Detection

3.1 Sensor fault model

When there are no faults, the linearized models of (10) and (12) can be rewritten as following general expression.

$$\dot{\boldsymbol{x}}(t) = \boldsymbol{A}\,\boldsymbol{x}(t) + \boldsymbol{B}\,\boldsymbol{u}(t) \qquad (13)$$
$$\boldsymbol{y}(t) = \boldsymbol{C}\boldsymbol{x}(t) + \boldsymbol{D}\,\boldsymbol{u}(t) \qquad (14)$$

where $\boldsymbol{x}$, $\boldsymbol{u}$ and $\boldsymbol{y}$ are the state vector, input vector and measurement vector, respectively.

The faults can be induced from system degradation, actuator fail, and sensor fail. In this paper, sensor fault is considered. The sensor faults can be described by multiplication and bias. The measurement equation (13) with faults can be written as

$$\boldsymbol{y}_f(t) = \boldsymbol{F}_s(\boldsymbol{C}\boldsymbol{x}(t) + \boldsymbol{D}\,\boldsymbol{u}(t)) + \boldsymbol{f}_{so} \qquad (15)$$

where $\boldsymbol{y}_f$ is faulted output, $\boldsymbol{F}_s$ denotes multiplication type fault and $\boldsymbol{f}_{so}$ bias type fault. When there are scale factor error in sensor, multiplication and bias type faults exist. It is because the output in linear system in (14) is calculated from

$$\boldsymbol{y}(t) = \boldsymbol{y}_{nonlinear}(t) - \boldsymbol{y}_{trim}$$

and if there exist scale factor faults, the faulted output in (15) will be

$$\begin{aligned} \boldsymbol{y}_f(t) &= \boldsymbol{K}\boldsymbol{y}_{nonlinear}(t) - \boldsymbol{y}_{trim} \\ &= \boldsymbol{K}(\boldsymbol{y}_{nonlinear}(t) - \boldsymbol{y}_{trim}) + (\boldsymbol{K}-1)\boldsymbol{y}_{trim} \\ &= \boldsymbol{K}\boldsymbol{y}(t) + (\boldsymbol{K}-1)\boldsymbol{y}_{trim} \end{aligned}$$

where $\boldsymbol{K}$ is a wrong scale factor in case $\boldsymbol{K} \neq 1$. When there are bias in sensor, only the bias type faults exist in (15).

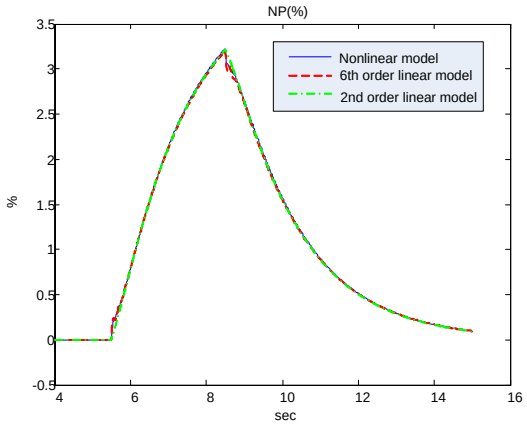

Fig. 5 Responses of combined models

3.2 SVD based fault detection method

The singular value decomposition(SVD) has been used to describe the characteristics of multi input multi output linear systems in frequency domain[8]. The SVD is used to detect faults of linear systems.

The singular value of $n \times m$ matrix $\boldsymbol{A}$ is defined as

$$\sigma_i(\boldsymbol{A}) = \sqrt{\lambda_i(\boldsymbol{A}^H\boldsymbol{A})} = \sqrt{\lambda_i(\boldsymbol{A}\boldsymbol{A}^H)} > 0$$

where σ_i is i-th singular value and λ_i is i-th nonzero eigenvalue. The σ_i's are sorted to satisfy following order

$$\sigma_1 > \sigma_2 > \sigma_3 \cdots$$

Then $\boldsymbol{A}$ can be decomposed as

$$\boldsymbol{A} = \boldsymbol{U}\boldsymbol{\Sigma}\boldsymbol{V}^H = \sum_{i=1}^{k} \sigma_i(\boldsymbol{A})\boldsymbol{u}_i\boldsymbol{v}_i^H.$$

where $\boldsymbol{\Sigma}$ is a diagonal matrix which consists of singular values, $\boldsymbol{U}$ is left singular vector matrix, and $\boldsymbol{V}$ is right singular vector matrix. The singular vector matrices are unitary matrix, that is $\boldsymbol{U}^H = \boldsymbol{U}^{-1}$ and $\boldsymbol{V}^H = \boldsymbol{V}^{-1}$. $\boldsymbol{u}_i$ and $\boldsymbol{v}_i$ denote i-th column vector of $\boldsymbol{U}$ and $\boldsymbol{V}$ respectively.

The frequency response of a system is considered to apply the SVD in fault detection. The frequency response of system (13) and (14) is

$$\boldsymbol{G}(j\omega) = \boldsymbol{C}(j\omega I - \boldsymbol{A})^{-1}\boldsymbol{B} + \boldsymbol{D} \qquad (16)$$

For a single input linear time invariant system, if $\sin\omega t$ is applied as an input the output will be

$$y(t) = |G(j\omega)| \sin(\omega t + \angle G(j\omega)) \qquad (17)$$

This result can be extended to multi input multi output system.

The SVD of $\boldsymbol{G}(j\omega)$ is represented as

$$\boldsymbol{G}(j\omega) = \boldsymbol{U}(j\omega)\boldsymbol{\Sigma}(\omega)\boldsymbol{V}^H(j\omega) \qquad (18)$$

Since $\boldsymbol{G}(j\omega)$ is known, the $\boldsymbol{U}(j\omega)$, $\boldsymbol{V}(j\omega)$, and $\boldsymbol{\Sigma}(j\omega)$ are also known. If $\boldsymbol{v}_i(j\omega)\, e^{j\omega t}$ is applied to the system as an input, the output will be

$$\begin{aligned} \boldsymbol{y}(t) &= \boldsymbol{U}(j\omega)\boldsymbol{\Sigma}(\omega)\ \boldsymbol{V}^H(j\omega)\boldsymbol{v}_i(j\omega)e^{j\omega t} \\ &= \boldsymbol{u}_i(j\omega)\sigma_i(\omega)\, e^{j\omega t} \end{aligned} \qquad (19)$$

The relation $\boldsymbol{V}^H = \boldsymbol{V}^{-1}$ is used in (19). The m-th element $y_m(t)$ of output vector $\boldsymbol{y}(t)$ is

$$\frac{y_m(t)}{\sigma_i(\omega)} = |u_{i,m}(j\omega)| \sin(\omega t + \angle u_{i,m}(j\omega)) \qquad (20)$$

If faults exist, (20) will be distorted as

$$\frac{y_m(t)}{\sigma_i(\omega)} = M_{i,m} \sin(\omega t + \Theta_{i,m}) + B_{i,m} \qquad (21)$$

where $M_{i,m}$, $\Theta_{i,m}$ and $B_{i,m}$ are amplitude, phase and bias of the distorted sine function and they are calculated from output and known $\sigma_i(\omega)$. If $M_{i,m} = |u_{i,m}(j,\omega)|$, $\Theta_{i,m} = \angle u_{i,m}(j,\omega)$ and $B_{i,m} = 0$, there are no faults, otherwise there exist faults related to m-th measurement.

The SVD method does not need calculating the residuals because it uses the characteristics that the system outputs in direction of the left singular vector if an input is applied in direction of the right singular vector. However, it is noted that the SVD method require a periodic input signal to obtain the frequency response of a system at a fixed frequency.

3.3 Simulation

Some simulations are performed to verify the performance of SVD based fault detection in FADEC system. The frequency of input is chosen as 10 rad/sec and hence the fuel flow is expressed as

$$W_f(t) = 0.001 * W_{f,trim} * \sin(10t) + W_{f,trim}$$

,where $W_{f,trim}$ means the fuel flow at trimmed condition. Then the output will be also an periodic signal and the frequency will be the same as input frequency.

Engine model combined with rotor dynamics at trim is described by one of linear systems (10) or (12). (10) or (12) is the reference model of SVD based fault detection. Measurements are acquired from the nonlinear engine and rotor combined model.

Fig. 6 ~ fig. 10 show $M_{i,m}$, $\Theta_{i,m}$ and $B_{i,m}$ for each faults. The results of the system without faults are displayed in fig. 6 and show $M_{i,m} = |u_{i,m}(j,\omega)|$, $\Theta_{i,m} = \angle u_{i,m}(j,\omega)$ and $B_{i,m} = 0$. The results for the models without and with rotor dynamics are almost same. The reason is that as shown in fig. 5 the responses of the two models are almost same since the rotor dynamics is very fast, Therefore, from now, we discuss the results of the model without rotor dynamics.

Consider the case when there is 10% scale factor fault in N_P. As shown in fig. 7, the $M_{i,m}$, $\Theta_{i,m}$ and $B_{i,m}$ associated with N_P fluctuates and other values are the same as them of normal system. Fig. 8 shows the results when there is 10% scale factor fault in N_G. In this case the $M_{i,m}$, $\Theta_{i,m}$ and $B_{i,m}$ corresponding to N_G only fluctuates. For the bias type faults with magnitude of 10% of trimmed value as shown in fig. 9(N_P bias) and fig. 10(N_G bias), the result show the same trend. Moreover it is possible to distinguish the scale factor faults and bias faults as shown in fig. 11 in which the $M_{i,m}$ for N_P in case N_P bias faults is same as that of without faults but different from that of scale factor faults. Similarly the SVD work well in all other sensor bias fault. Summarizing the simulation results, the SVD based method can detect the occurrence of fault and moreover identify the sensor faulted and the types of faults.

4. Conclusions

A linearized engine model including rotor dynamics was constructed for the T700-GE-700 turboshaft engine powering UH-60 helicopter. Simulation showed effects of flapping and lagging motion in the transient phase of the power turbine dynamics.

The singular value decomposition(SVD) method was applied to the developed model in order to detect sensor faults. Simulations showed that the SVD method worked well in detecting and isolating the sensor faults.

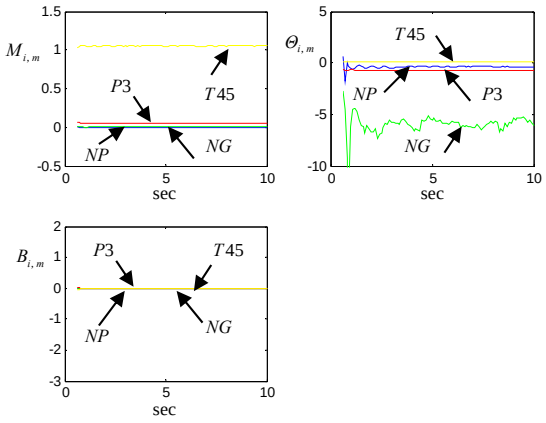

(a) with rotor dynamics

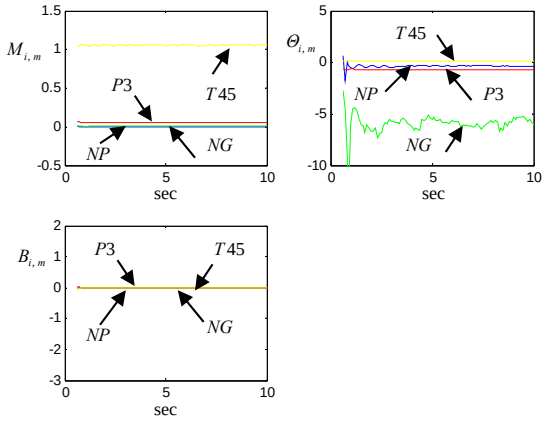

(b) without rotor dynamics

Fig. 6 $M_{i,m}$, $\Theta_{i,m}$ and $B_{i,m}$ of normal system

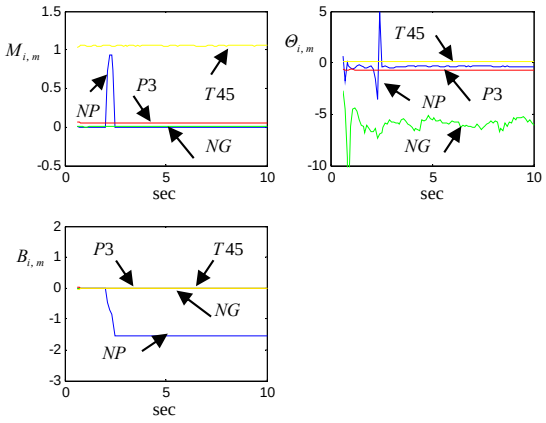

Fig. 7 $M_{i,m}$, $\Theta_{i,m}$ and $B_{i,m}$ of N_P 10% scale factor fault

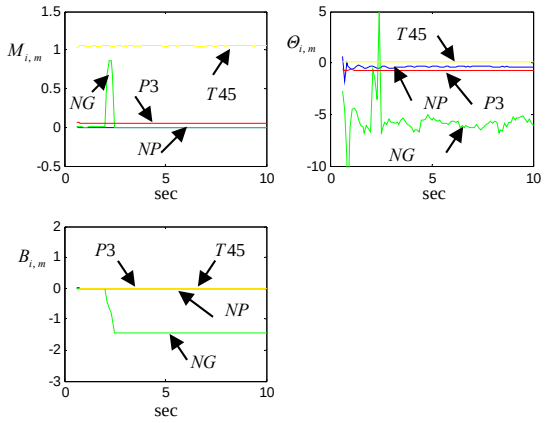

Fig. 8 $M_{i,m}$, $\Theta_{i,m}$ and $B_{i,m}$ of N_G 10% scale factor fault

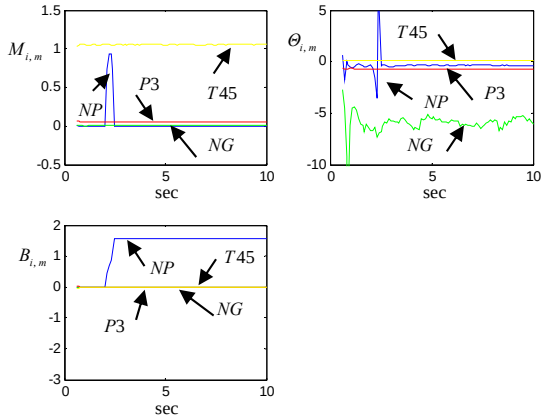

Fig. 9 $M_{i,m}$, $\Theta_{i,m}$ and $B_{i,m}$ of N_P 10% bias fault

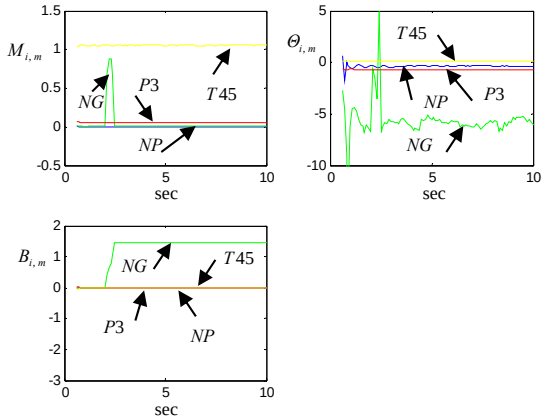

Fig. 10 $M_{i,m}$, $\Theta_{i,m}$ and $B_{i,m}$ of N_G 10% bias fault

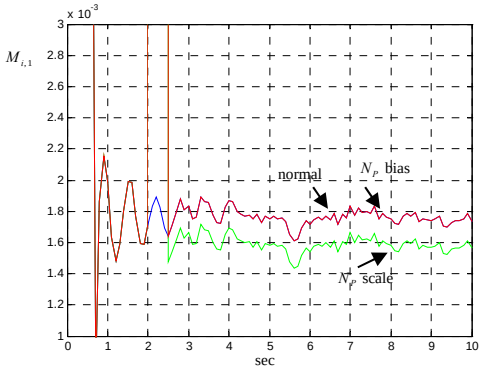

Fig. 11 $M_{i,m}$ for N_P in case without, N_P scale factor and N_P bias faults

Acknowledgement

This study has been supported by the KARI under KHP Dual-Use Component Development Program funded by the MOCIE.

References

[1] M. G. Ballin, "A High Fidelity Real-Time Simulation of a Small Turboshaft Engine," NASA TM 100991, 1988.

[2] S. Newman, The Foundation of Helicopter Flight, Edward Arnold, 1994.

[3] R. Isermann, "Model-based fault detection and diagnosis - status and applications," *IFAC*, Symposium on Automatic control in Aerospace 2004

[4] Sang Man Seong, Ihn Seok Lee, "SVD Based Sensor Fault Isolation for Small Turbo Shaft Engine," Proceeding of the 2007 KSAS Autumn Conference, Korea, 2007

[5] J. J. Howlett, "UH-60A Black Hawk Engineering Simulation Program: Vol. I - Mathematical Model," NASA CR 166309, 1981.

[6] R. E. Maine and K. W. Iliff, "User's Manual for MMLE3, a General FORTRAN Program for Maximum Likelihood Parameter Estimation," NASA TP 1563, 1980.

[7] T. Kailath, Linear Systems, Prentice Hall, Inc., 1980.

[8] K. Zbou, J. C. Doyle, and K. Glover, Robust and Optimal Control, Prentice Hall, Inc., 1996.